Deep Inelastic Scattering Events with a Large Rapidity Gap at HERA

H1 Collaboration

Abstract

Evidence is presented using data taken with the H1 detector at HERA for a class of deep inelastic electron–proton scattering (DIS) events ($5 < Q^2 < 120\,GeV^2$) at low Bjorken-x ($10^{-4} < x < 10^{-2}$) which have almost no hadronic energy flow in a large interval of pseudo-rapidity around the proton remnant direction and which cannot be attributed to our present understanding of DIS and fluctuations in final state hadronic fragmentation. From an integrated luminosity of $273\,nb^{-1}$, 734 events, that is about 5% of the total DIS sample, have no energy deposition greater than $400\,MeV$ forward of laboratory pseudo-rapidity $\eta_{max} = 1.8$ up to the largest measurable pseudo-rapidity of about 3.65. Evidence that about 10% of observed rapidity gap events are exclusive vector meson electroproduction is presented. Good descriptions of the data are obtained using models based either on a vector meson dominance like picture, which includes a large fraction of inelastic virtual photon dissociation, or on deep inelastic electron–pomeron scattering in which the partonic sub–structure of the latter is resolved.

H1 Collaboration

T. Ahmed[3], S. Aid[13], V. Andreev[24], B. Andrieu[28], R.-D. Appuhn[11], M. Arpagaus[36],
A. Babaev[26], J. Baehr[35], J. Bán[17], P. Baranov[24], E. Barrelet[29], W. Bartel[11], M. Barth[4],
U. Bassler[29], H.P. Beck[37], H.-J. Behrend[11], A. Belousov[24], Ch. Berger[1], H. Bergstein[1],
G. Bernardi[29], R. Bernet[36], G. Bertrand-Coremans[4], M. Besançon[9], P. Biddulph[22],
J.C. Bizot[27], V. Blobel[13], K. Borras[8], F. Botterweck[4], V. Boudry[28], A. Braemer[14], F. Brasse[11],
W. Braunschweig[1], V. Brisson[27], D. Bruncko[17], C. Brune[15], R.Buchholz[11], L. Büngener[13],
J. Bürger[11], F.W. Büsser[13], A. Buniatian[11,39], S. Burke[18], G. Buschhorn[26], A.J. Campbell[11],
T. Carli[26], F. Charles[11], D. Clarke[5], A.B. Clegg[18], B. Clerbaux[4], M. Colombo[8],
J.G. Contreras[8], J.A. Coughlan[5], A. Courau[27], Ch. Coutures[9], G. Cozzika[9], L. Criegee[11],
D.G. Cussans[5], J. Cvach[30], S. Dagoret[29], J.B. Dainton[19], M. Danilov[23], W.D. Dau[16],
K. Daum[34], M. David[9], E. Deffur[11], B. Delcourt[27], L. Del Buono[29], A. De Roeck[11],
E.A. De Wolf[4], P. Di Nezza[32], C. Dollfus[37], J.D. Dowell[3], H.B. Dreis[2], J. Duboc[29],
D. Düllmann[13], O. Dünger[13], H. Duhm[12], J. Ebert[34], T.R. Ebert[19], G. Eckerlin[11],
V. Efremenko[23], S. Egli[37], H. Ehrlichmann[35], S. Eichenberger[37], R. Eichler[36], F. Eisele[14],
E. Eisenhandler[20], R.J. Ellison[22], E. Elsen[11], M. Erdmann[14], E. Evrard[4], L. Favart[4],
A. Fedotov[23], D. Feeken[13], R. Felst[11], J. Feltesse[9], J. Ferencei[15], F. Ferrarotto[32], K. Flamm[11],
M. Fleischer[11], M. Flieser[26], G. Flügge[2], A. Fomenko[24], B. Fominykh[23], M. Forbush[7],
J. Formánek[31], J.M. Foster[22], G. Franke[11], E. Fretwurst[12], E. Gabathuler[19], K. Gabathuler[33],
K. Gamerdinger[26], J. Garvey[3], J. Gayler[11], M. Gebauer[8], A. Gellrich[13], H. Genzel[1],
R. Gerhards[11], U. Goerlach[11], L. Goerlich[6], N. Gogitidze[24], M. Goldberg[29], D. Goldner[8],
B. Gonzalez-Pineiro[29], A.M. Goodall[19], I. Gorelov[23], P. Goritchev[23], C. Grab[36], H. Grässler[2],
R. Grässler[2], T. Greenshaw[19], G. Grindhammer[26], A. Gruber[26], C. Gruber[16], J. Haack[35],
D. Haidt[11], L. Hajduk[6], O. Hamon[29], M. Hampel[1], E.M. Hanlon[18], M. Hapke[11], W.J. Haynes[5],
J. Heatherington[20], V. Hedberg[21], G. Heinzelmann[13], R.C.W. Henderson[18], H. Henschel[35],
R. Herma[1], I. Herynek[30], M.F. Hess[26], W. Hildesheim[12], P. Hill[5], K.H. Hiller[35], C.D. Hilton[22],
J. Hladký[30], K.C. Hoeger[22], M. Höppner[8], R. Horisberger[33], Ph. Huet[4], H. Hufnagel[14],
M. Ibbotson[22], H. Itterbeck[1], M.-A. Jabiol[9], A. Jacholkowska[27], C. Jacobsson[21], M. Jaffre[27],
J. Janoth[15], T. Jansen[11], L. Jönsson[21], K. Johannsen[13], D.P. Johnson[4], L. Johnson[18],
H. Jung[11], P.I.P. Kalmus[20], D. Kant[20], R. Kaschowitz[2], P. Kasselmann[12], U. Kathage[16],
H.H. Kaufmann[35], S. Kazarian[11], I.R. Kenyon[3], S. Kermiche[27], C. Keuker[1], C. Kiesling[26],
M. Klein[35], C. Kleinwort[13], G. Knies[11], W. Ko[7], T. Köhler[1], H. Kolanoski[8], F. Kole[7],
S.D. Kolya[22], V. Korbel[11], M. Korn[8], P. Kostka[35], S.K. Kotelnikov[24], M.W. Krasny[6,29],
H. Krehbiel[11], D. Krücker[2], U. Krüger[11], U. Krüner-Marquis[11], J.P. Kubenka[26], H. Küster[2],
M. Kuhlen[26], T. Kurča[17], J. Kurzhöfer[8], B. Kuznik[34], D. Lacour[29], F. Lamarche[28], R. Lander[7],
M.P.J. Landon[20], W. Lange[35], P. Lanius[26], J.-F. Laporte[9], A. Lebedev[24], C. Leverenz[11],
S. Levonian[11,24], Ch. Ley[2], A. Lindner[8], G. Lindström[12], F. Linsel[11], J. Lipinski[13], B. List[11],
P. Loch[27], H. Lohmander[21], G.C. Lopez[20], D. Lüke[8,11], N. Magnussen[34], E. Malinovski[24],
S. Mani[7], R. Maraček[17], P. Marage[4], J. Marks[25], R. Marshall[22], J. Martens[34], R. Martin[19],
H.-U. Martyn[1], J. Martyniak[6], S. Masson[2], T. Mavroidis[20], S.J. Maxfield[19], S.J. McMahon[19],
A. Mehta[22], K. Meier[15], D. Mercer[22], T. Merz[11], C.A. Meyer[37], H. Meyer[34], J. Meyer[11],
S. Mikocki[6], D. Milstead[19], F. Moreau[28], J.V. Morris[5], G. Müller[11], K. Müller[37], P. Murín[17],
V. Nagovizin[23], R. Nahnhauer[35], B. Naroska[13], Th. Naumann[35], P.R. Newman[3], D. Newton[18],
D. Neyret[29], H.K. Nguyen[29], F. Niebergall[13], C. Niebuhr[11], R. Nisius[1], G. Nowak[6],
G.W. Noyes[5], M. Nyberg-Werther[21], H. Oberlack[26], U. Obrock[8], J.E. Olsson[11], E. Panaro[12],
A. Panitch[4], C. Pascaud[27], G.D. Patel[19], E. Peppel[11], E. Perez[9], J.P. Phillips[22], Ch. Pichler[12],
D. Pitzl[36], G. Pope[7], S. Prell[11], R. Prosi[11], G. Rädel[11], F. Raupach[1], P. Reimer[30],
S. Reinshagen[11], P. Ribarics[26], V. Riech[12], J. Riedlberger[36], S. Riess[13], M. Rietz[2],
S.M. Robertson[3], P. Robmann[37], H.E. Roloff[35], R. Roosen[4], K. Rosenbauer[1] A. Rostovtsev[23],
F. Rouse[7], C. Royon[9], K. Rüter[26], S. Rusakov[24], K. Rybicki[6], R. Rylko[20], N. Sahlmann[2],
E. Sanchez[26], D.P.C. Sankey[5], M. Savitsky[23], P. Schacht[26], S. Schiek[11], P. Schleper[14],

W. von Schlippe[20], C. Schmidt[11], D. Schmidt[34], G. Schmidt[13], A. Schöning[11], V. Schröder[11], E. Schuhmann[26], B. Schwab[14], A. Schwind[35], U. Seehausen[13], F. Sefkow[11], M. Seidel[12], R. Sell[11], A. Semenov[23], V. Shekelyan[23], I. Sheviakov[24], H. Shooshtari[26], L.N. Shtarkov[24], G. Siegmon[16], U. Siewert[16], Y. Sirois[28], I.O. Skillicorn[10], P. Smirnov[24], J.R. Smith[7], Y. Soloviev[24], H. Spitzer[13], R. Starosta[1], M. Steenbock[13], P. Steffen[11], R. Steinberg[2], B. Stella[32], K. Stephens[22], J. Stier[11], J. Stiewe[15], U. Stösslein[35], J. Strachota[30], U. Straumann[37], W. Struczinski[2], J.P. Sutton[3], S. Tapprogge[15], R.E. Taylor[38,27], V. Tchernyshov[23], C. Thiebaux[28], G. Thompson[20], I. Tichomirov[23], P. Truöl[37], J. Turnau[6], J. Tutas[14], P. Uelkes[2], A. Usik[24], S. Valkár[31], A. Valkárová[31], C. Vallée[25], P. Van Esch[4], P. Van Mechelen[4], A. Vartapetian[11,39], Y. Vazdik[24], M. Vecko[30], P. Verrecchia[9], G. Villet[9], K. Wacker[8], A. Wagener[2], I.W. Walker[18], A. Walther[8], G. Weber[13], M. Weber[11], D. Wegener[8], A. Wegner[11], H.P. Wellisch[26], L.R. West[3], S. Willard[7], M. Winde[35], G.-G. Winter[11], Th. Wolff[36], A.E. Wright[22], E. Wünsch[11], N. Wulff[11], T.P. Yiou[29], J. Žáček[31], Z. Zhang[27], M. Zimmer[11], W. Zimmermann[11], F. Zomer[27], and K. Zuber[15]

[1] *I. Physikalisches Institut der RWTH, Aachen, Germany[a]*
[2] *III. Physikalisches Institut der RWTH, Aachen, Germany[a]*
[3] *School of Physics and Space Research, University of Birmingham, Birmingham, UK[b]*
[4] *Inter-University Institute for High Energies ULB-VUB, Brussels; Universitaire Instellingen Antwerpen, Wilrijk, Belgium[c]*
[5] *Rutherford Appleton Laboratory, Chilton, Didcot, UK[b]*
[6] *Institute for Nuclear Physics, Cracow, Poland[d]*
[7] *Physics Department and IIRPA, University of California, Davis, California, USA[e]*
[8] *Institut für Physik, Universität Dortmund, Dortmund, Germany[a]*
[9] *CEA, DSM/DAPNIA, CE-SACLAY, Gif-sur-Yvette, France*
[10] *Department of Physics and Astronomy, University of Glasgow, Glasgow, UK[b]*
[11] *DESY, Hamburg, Germany[a]*
[12] *I. Institut für Experimentalphysik, Universität Hamburg, Hamburg, Germany[a]*
[13] *II. Institut für Experimentalphysik, Universität Hamburg, Hamburg, Germany[a]*
[14] *Physikalisches Institut, Universität Heidelberg, Heidelberg, Germany[a]*
[15] *Institut für Hochenergiephysik, Universität Heidelberg, Heidelberg, Germany[a]*
[16] *Institut für Reine und Angewandte Kernphysik, Universität Kiel, Kiel, Germany[a]*
[17] *Institute of Experimental Physics, Slovak Academy of Sciences, Košice, Slovak Republic*
[18] *School of Physics and Materials, University of Lancaster, Lancaster, UK[b]*
[19] *Department of Physics, University of Liverpool, Liverpool, UK[b]*
[20] *Queen Mary and Westfield College, London, UK[b]*
[21] *Physics Department, University of Lund, Lund, Sweden[f]*
[22] *Physics Department, University of Manchester, Manchester, UK[b]*
[23] *Institute for Theoretical and Experimental Physics, Moscow, Russia*
[24] *Lebedev Physical Institute, Moscow, Russia*
[25] *CPPM, Université d'Aix-Marseille II, IN2P3-CNRS, Marseille, France*
[26] *Max-Planck-Institut für Physik, München, Germany[a]*
[27] *LAL, Université de Paris-Sud, IN2P3-CNRS, Orsay, France*
[28] *LPNHE, Ecole Polytechnique, IN2P3-CNRS, Palaiseau, France*
[29] *LPNHE, Universités Paris VI and VII, IN2P3-CNRS, Paris, France*
[30] *Institute of Physics, Czech Academy of Sciences, Praha, Czech Republic[g]*
[31] *Nuclear Center, Charles University, Praha, Czech Republic[g]*
[32] *INFN Roma and Dipartimento di Fisica, Universita "La Sapienza", Roma, Italy*
[33] *Paul Scherrer Institut, Villigen, Switzerland*
[34] *Fachbereich Physik, Bergische Universität Gesamthochschule Wuppertal, Wuppertal, Germany[a]*
[35] *DESY, Institut für Hochenergiephysik, Zeuthen, Germany[a]*

[36] *Institut für Teilchenphysik, ETH, Zürich, Switzerland[h]*

[37] *Physik-Institut der Universität Zürich, Zürich, Switzerland[h]*

[38] *Stanford Linear Accelerator Center, Stanford California, USA*

[39] *Visitor from Yerevan Phys.Inst., Armenia*

1 Introduction

The electron–proton (ep) collider HERA, in which $26.7\,GeV$ electrons collide with $820\,GeV$ protons, not only enables the extension of the kinematic range of measurements in the deep inelastic scattering (DIS) of electrons and protons but also opens up new possibilities for the study of the hadronic final state. Due to the large ep centre of mass energy $\sqrt{s} = 296\,GeV$, for the first time measurements of DIS are possible with substantial Q^2 (the space-like boson invariant mass squared $\geq 5\,GeV^2$) at very low Bjorken–$x \leq 10^{-3}$. Bjorken-x is defined by $x = \frac{Q^2}{2p.q}$ where p is the four momentum of the incoming proton and q that of the virtual boson. In this low x kinematic region, modifications to the leading order parton model picture of DIS are likely to be substantial, which could mean that our present interpretation of DIS in such terms is inadequate.

In the following a coordinate system is used with origin at the interaction point and z axis along the proton beam, or forward, direction. The pseudo-rapidity of a final state particle with polar angle θ is then $\eta = -\ln\tan(\frac{\theta}{2})$.

For the majority of DIS events the final state hadronic energy flow is spread between the directions of the struck parton and the proton remnant. Due to the high incident proton momentum at HERA, the directions of these two systems are generally very different in the laboratory. Hence detailed studies of the energy flow associated with them and their inter–relation become possible. First results of such studies have shown that the main features of the energy flow around the direction of the struck parton are well reproduced by various "standard DIS" models in which ep scattering is explained in terms of the interaction of a virtual electroweak boson with the partonic content of the proton. The energy flow in the region around the proton remnant is however less well described [1]. In particular the ZEUS collaboration have reported an excess ($\sim 7\%$ to 8%, $Q^2 > 10\,GeV^2$, $W > 140\,GeV$) over the expectations of standard DIS models of events in which no energy flow is observed in a large region of pseudo–rapidity close to the proton direction, specifically from the start of detector acceptance to $\eta = 1.5$ [2]. Standard DIS models describe the main features of hadronic energy flow in DIS as being a consequence of the chromodynamic radiation from the colour charges exchanged in the interaction. The observation of deep inelastic ep rapidity gap events may indicate that the virtual photon interacts with the proton with no exchange of colour. The substantial Q^2 of the interaction suggests that the sub-structure of the colourless exchange may be resolved, or that its spatial extent is small. The similarity of the Q^2 dependence of the yields of rapidity gap and all DIS events, for total hadronic invariant mass $W > 140\,GeV$, is interpreted as evidence for a leading twist QCD production mechanism.

In this paper we describe the observation of rapidity gap events using the H1 detector at the HERA collider at DESY, Hamburg. Preliminary studies of these events, based on an integrated ep luminosity of $22.5\,nb^{-1}$, were reported in July 1993 [3]. Two rapidity gap events are shown in figure 1. In the first there is energy deposition throughout the detector, except in the forward region, and large charged particle multiplicity in the central charged track detectors. In the second the observed hadronic final state consists of two oppositely charged particles, the p_T of which balances that of the scattered electron. In both cases the electron is detected in the backward region of H1.

Here we make a first comparison with our data of models based on the assumption that the proton interacts diffractively. The interaction may therefore be modelled as the (colourless) exchange of a t-channel Regge pole, the pomeron. Two mechanisms are considered.

The first mechanism is motivated by the possibility that rapidity gap events are attributable to processes which do not involve the spatial separation of coloured pomeron partonic sub-structure, and thus in which there is no coloured remnant left from the virtual photon–pomeron
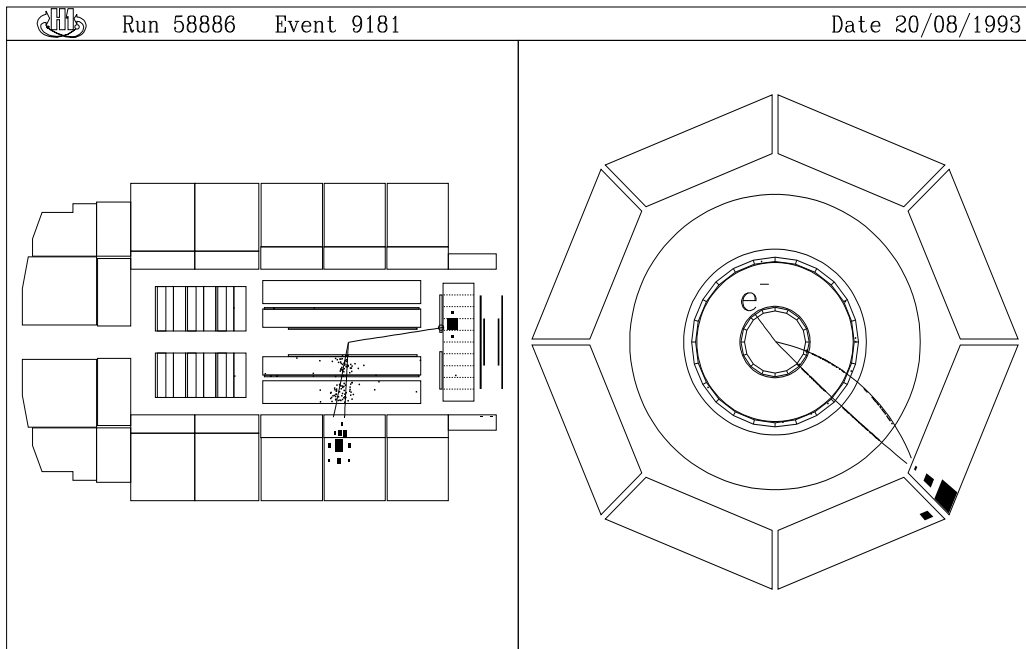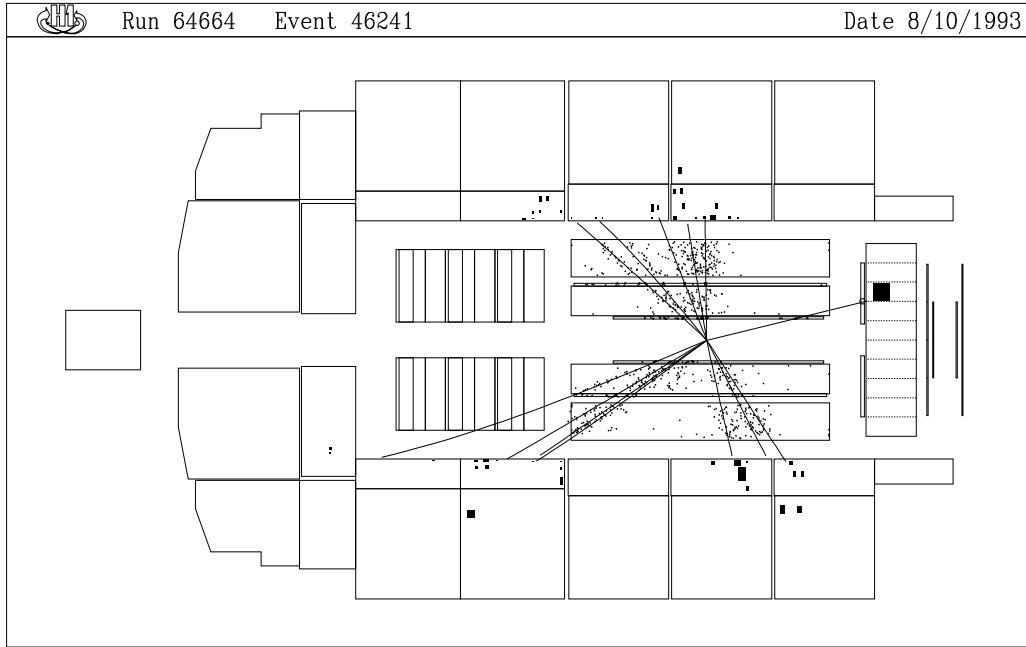
e⁻

Figure 1: Two DIS events observed with the H1 detector in which a large region around the proton direction (to the left) is devoid of energy flow; $820\,GeV$ protons are incident from the right, $26.7\,GeV$ electrons from the left; the upper ((r,z) view only) has widely distributed hadronic energy flow in the "barrel" region of the liquid argon calorimeter which is spatially associated with high charged track multiplicity in the CTD and not in the FTD; the lower ((r,z) and (r,ϕ) views) contains two oppositely charged tracks in the CTD with associated calorimeter energy. For explanation of the detector components see the text.

interaction. An example is the observation of exclusive vector meson (VM) leptoproduction at significant Q^2 [4, 5]. Different theoretical approaches to exclusive VM leptoproduction exist, based on vector meson dominance (VMD) of the photon [6], and on QCD or partonic models [7]. Inelastic interactions of the virtual photon in such a mechanism can be modelled conveniently in the framework of VMD, or taken to follow a partonic description such as that in the "aligned jet model" [8] which is expected to be significant in ep DIS at low Bjorken$-x$. We here adopt a phenomenological approach, based on VMD, to build a model which provides a feasible way of comparing our data with both elastic and inelastic interactions of this type.

The second mechanism considers the possibility that any partonic sub-structure of the pomeron is resolved and interacts solely with the high Q^2 photon, that is deep inelastic electron–pomeron scattering, and in which there may exist a coloured pomeron remnant from the interaction.

2   The H1 Detector and DIS Event Selection

The data on which the work described here is based were taken with the H1 detector at the HERA ep collider at DESY in Hamburg and correspond to an integrated luminosity of $273\,nb^{-1}$. The H1 detector is described in detail in [9]. The components of particular importance to this analysis are as follows (see figure 1).

The backward electromagnetic calorimeter (BEMC) measures the energy of electrons scattered into the backward region of H1 with an accuracy of $\frac{\sigma_E}{E} \sim \frac{10\%}{\sqrt{E\,GeV}}$ and with an overall (electromagnetic) energy scale known to within 2% in this data sample. The backward region corresponds to small angle electron scattering, that is for HERA the low Q^2 region. The BEMC covers the angular range $156° < \theta < 174°$ which corresponds to $120 > Q^2 > 5\,GeV^2$ with a minimum measured electron energy of $12\,GeV$.

Immediately in front of the BEMC is the backward proportional chamber (BPC), which determines the point at which charged particles enter the BEMC with an accuracy of a few millimetres over all but its outermost regions, where this function is taken over by the central track detector (CTD, see below). For events in which a z vertex is determined, the resulting polar angle measurement is accurate to $\sigma \sim 2\,mrad$.

The time-of-flight system (TOF), placed behind the BEMC, registers whether an energy deposit in the BEMC occurred outside the time window expected for a HERA ep collision, in which case the source was a proton beam wall or beam gas interaction within or before the detector.

The central tracking detectors (CTD) are a hybrid of inner and outer jet chambers (CJC), z drift chambers and proportional chambers. The proportional chambers provide a fast signal and allow H1 to trigger on tracks which originate from the z range expected for ep interactions.

The forward tracking detector (FTD) is an array of drift and proportional chambers which extend track measurement into the forward direction.

In off-line analysis, two sets of CJC track criteria were used. The first, for the definition of tracks used in the reconstruction of the event z vertex, required a minimum of 5 hits in the CJC. The second, to define tracks used in the analysis of the final state, required a minimum of 10 CJC hits. The mass resolution for meson decays to $\pi^+\pi^-$ using the latter track definition is then typically $\sigma \sim 20\,MeV$, as confirmed by observation of K_S^0 decay in our DIS sample. The track criteria used in the FTD were a minimum of 9 hits and a momentum of at least $0.4\,GeV$ for the reconstruction of the z vertex. Tracks used in the final state analysis were required to have a minimum of 18 hits.

The liquid argon calorimeter is divided into electromagnetic and hadronic sections, with lead and steel absorber respectively [10]. Hadronic energy is measured with an accuracy of $\frac{\sigma_E}{E} \sim \frac{50\%}{\sqrt{E\,GeV}}$ as shown by test beam measurements and, for the data studied here, with an overall energy scale known to within 6%. The liquid argon calorimeter is finely segmented, enabling accurate determination of the pseudo-rapidity η of energy deposited within it. In the forward region, extending to $\eta \sim 3.65$, the granularity is such that the polar angle which is subtended at the event vertex by energy deposits in individual cells is $\leq 15\,mrad$.

An as yet only partially instrumented copper silicon calorimeter, the plug, extends calorimetric coverage in the forward direction to a pseudo-rapidity of $\eta = 5.2$.

The iron yoke of the solenoid magnet which provides the uniform magnetic field for the H1 tracking detectors is interleaved with limited streamer tubes for the measurement both of hadronic energy flow leaking out of the liquid argon calorimeter and of penetrating muons. The coverage of this muon system extends throughout the central region into the forward region to $\eta = 3.35$.

The forward muon spectrometer (Fμ) enhances muon identification and measurement in the forward region of H1 ($1.90 < \eta < 3.64$). In addition, forward going hadronic energy in the pseudo-rapidity range $5.0 < \eta < 6.6$ may produce charged particles by secondary interactions in the collimators, beam pipe and adjacent material which are detected in the Fμ drift chambers.

The forward proton tagger (P$_{tag}$) consists of two layers, each composed of scintillator sheets sandwiched by lead shielding. It is situated $24\,m$ from the interaction point in the proton direction and the scintillator sheets cover an area of about $60 \times 60\,cm^2$ transverse to and around the beam pipes. The resulting coverage in pseudo-rapidity is $5.8 < \eta < 8$. When used in conjunction with Fμ and the plug calorimeter, P$_{tag}$ is able to identify charged multiplicity associated with forward energy flow in this rapidity range.

Electrons and photons emitted at very small angles to the electron beam direction are detected in two electromagnetic calorimeters (Lumi) located $33\,m$ and $103\,m$ from the interaction point in the electron direction. Designed to measure luminosity by detecting $e\gamma$ coincidences from elastic radiative ep collisions, they are in addition used here to help quantify background due to photoproduction.

The data used here were obtained with a trigger requiring the presence of a localized energy cluster in the BEMC of $4\,GeV$ or more. Studies using an independent z vertex track trigger indicate that this trigger is 100% efficient for events in which an electron of energy $10\,GeV$ or more enters the BEMC. A selection, similar to that used to define the data sample described in [11], required the identification of a scattered electron in the BEMC as follows. The energy deposit was required to be electromagnetic in character, to not occur outside the TOF time window expected for an ep interaction, and to be associated with a hit in the BPC directly in front of the BEMC or with a track in the CTD. It was also required that an event z vertex be reconstructed from at least one track and that it lie within $35\,cm$ of the nominal interaction point. The majority of hits in the CTD were required to be associated with tracks from the event vertex, thereby suppressing events with tracks resulting from beam wall or gas interactions. The energy of the scattered electron was required to be at least $12\,GeV$ and its polar angle θ to be less than 172.5°. A total of 14550 events satisfied these criteria.

Studies, using various Monte Carlo simulations and using events in which an electron was detected in the luminosity system, indicate that the data sample selected as above consists overwhelmingly of DIS events [11]. The remaining $\sim 3\%$ background are due primarily to γp interactions in which early showering pions fake the electron signature in the BEMC and are concentrated at low scattered electron energies.

7

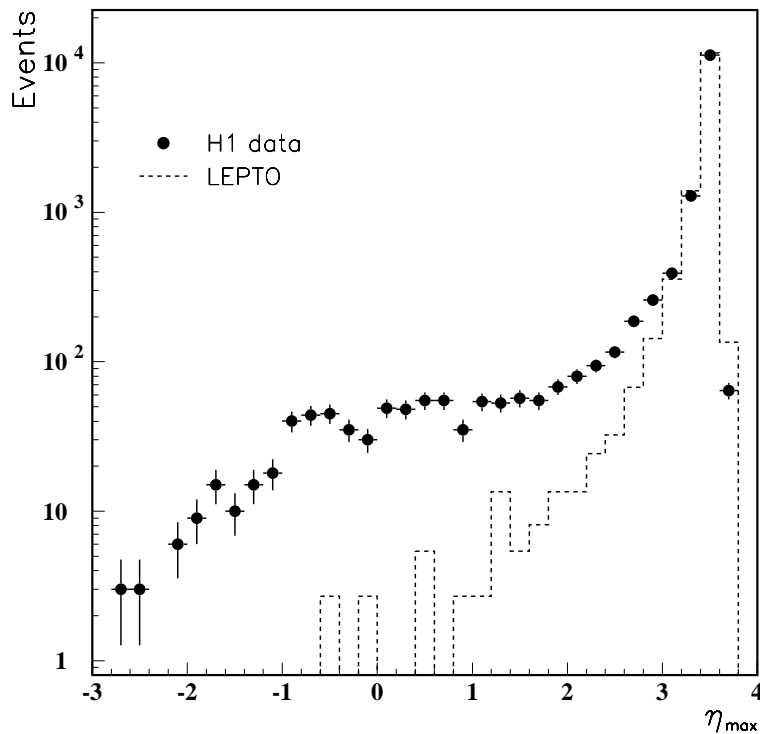Figure 2: Distribution of measured η_{max} for all DIS events together with the expectation from the "standard DIS" model (see text) based on the LEPTO simulation.

3 Selection of Rapidity Gap Events and Background Studies

The largest pseudo-rapidity which may be measured in the H1 liquid argon calorimeter, η_{LAr}, is about 3.65, and varies slightly due to the position of the ep event vertex. We define η_{max} for each event to be the largest pseudo-rapidity for which the summed energy deposited in the liquid argon and backward electromagnetic calorimeter cells in a cone about the forward proton direction with $\eta > \eta_{max}$ is at least $E_{min} = 0.4\,GeV$. A histogram of η_{max} for all DIS events, figure 2, reveals that, in most events, there is energy close to η_{LAr}. There is also a class of events in which there is a large pseudo-rapidity gap adjacent to η_{LAr}, which is not expected in the standard DIS models discussed above. This observation is not affected by varying E_{min} within the limits $0.3 < E_{min} < 0.6\,GeV$. A sample of events with large rapidity gap was selected from the DIS sample by requiring that $\eta_{max} < 1.8$. A total of 737 events, or 5% of the DIS sample, satisfied this criterion. Of these events, less than 2% had one or more charged particle with momentum greater than $0.4\,GeV$ reconstructed in the FTD in the angular range $4.6° < \theta < 18.8°$ $(3.2 > \eta > 1.8)$.

An alternative selection based on the use of energy clusters in the liquid argon calorimeter yielded similar results. Taking all clusters of energy greater than $0.4\,GeV$, and specifying their pseudo-rapidities by the centre of the energy cluster and the event vertex, we found 773 events in the DIS sample (5.3%) have no clusters above a laboratory pseudo-rapidity of 1.8. In all that follows we work with the former selection based on energy flow in cones of laboratory pseudo-rapidity.

Pile-up in the liquid argon calorimeter, in which energy deposited in earlier or later bunch crossings (HERA bunch crossing interval is 96 ns) contributes spurious forward energy deposition and therefore biases against the rapidity gap selection, was found to be insignificant.

8

The selection criteria above can also be satisfied by electron beam gas events in which beam electrons interact with the residual gas inside the beam pipe. An estimate of the level of this background in the rapidity gap sample was made using the so-called electron pilot bunches in HERA. The proton RF buckets which entered the interaction region in coincidence with these bunches were empty. Hence any interactions observed within the beam pipe were due to electron beam gas collisions. No such events were found in the rapidity gap sample. Taking into consideration the relative electron currents in colliding and pilot bunches, this implies an upper limit of 19 electron gas events in the rapidity gap sample (90% CL). Proton beam gas interactions do not contribute to the rapidity gap sample.

The level of background due to γp interactions in the rapidity gap sample was determined using those events in the sample in which an electron was detected in the Lumi detectors. The contamination was found to be similar to that in the entire DIS sample, namely $\sim 3\%$ [11]. The H1 muon system was used to check that the presence of cosmic ray interaction background in the rapidity gap sample was negligible. Extrapolation of the measured hadronic two photon cross section [12] show that two photon interactions do not contribute significantly to the rapidity gap sample ($\ll 1$ event). Three candidate Compton events ($ep \rightarrow ep\gamma$) were found in the rapidity gap sample and removed.

The rapidity gap sample considered below thus contains 734 events (5% of the total DIS sample). The number of events expected in this sample from standard DIS simulation is found to be between 12 and 53, where the uncertainty is a consequence of our current understanding of the proton structure functions and of parton fragmentation schemes.

4   Monte Carlo Models

The data were compared with the results of various Monte Carlo programs.

Deep inelastic ep scattering without colourless exchange was simulated using either LEPTO [13], which utilises $O(\alpha_S)$ matrix elements and parton showers, or a combination of LEPTO and ARIADNE [14] in which hadrons are radiated from a colour dipole. The parton distribution parameterisation used for the proton was MRSD- [15] which reproduces recent measurements of the proton structure function F_2 [11].

To model interactions in which any coloured sub-structure in ep interactions with a colourless exchange either is not resolved or is not spatially separated, the diffractive interaction of VM dominated, virtual photons with protons was simulated using a prescription based on measurements of hadronic photoproduction and lower Q^2 electroproduction [16, 17]. The virtual photon was taken to interact as a VM via pomeron exchange with the proton. A form factor $F(Q^2, y)$ dominated by a VM of mass m_V, namely

$$F(Q^2, y) = (\frac{1}{1 + \frac{Q^2}{m_V^2}})^2 [1 + \epsilon(y) R_{LT}(Q^2, y)] \tag{1}$$

was assumed, where $R_{LT}(Q^2, y)$ is the ratio of the longitudinal to transverse virtual photon-proton cross sections in the Lorentz frame in which the proton is at rest. The ratio of longitudinal to transverse virtual photon flux, as specified in QED, is given by

$$\epsilon(y) = \frac{2(1 - y)}{2(1 - y) + y^2} \tag{2}$$

where y is the DIS scaling variable $y = \frac{Q^2}{sx}$, and the Q^2 dependence of $\epsilon(y)$, which is very small in this frame, is neglected. $F(Q^2, y)$ is known to describe the Q^2 dependence of the elastic $\rho(770)$

component of hadronic leptoproduction at low Q^2 with $R_{LT} \propto Q^2$ [18]. Little is known about R_{LT} for the electroproduction of vector mesons on hydrogen at $Q^2 \geq 5\,GeV^2$ [1]. For simulation in the Q^2 range of the data presented here, we have adopted the ansatz

$$R_{LT} = \frac{\frac{Q^2}{m_V^2}}{1 + \frac{Q^2}{m_V^2}} \qquad (3)$$

which is consistent with the low Q^2 measurements, and at higher Q^2 does not permit the dominance of the large longitudinal scattering cross section from the low mass VMD contributions, namely $\rho(770)$, $\omega(783)$, and $\phi(1020)$. Note that for inelastic VMD–like processes, alternative choices for $F(Q^2, y)$ in equation 1 are possible [6] because very little is known about the Q^2 dependence of such dissociation. A phenomenological parameterisation of hadronic diffraction was used for the pomeron exchange [20, 21]. For elastic interactions (figure 3a) the resulting dependence on the four momentum transfer squared t of the virtual photon-proton interaction is $e^{\sim 10t}$ and for inelastic interactions $e^{\sim 5t}$ (figures 3b), 3c) and 3d)). Because we are unable to detect and reconstruct precisely either the scattered proton or its dissociated products using our present forward detectors, we are insensitive experimentally to the details of this t dependence. For inelastic interactions the dissociation of the VM or of the proton into a system of mass M is taken to follow a $\frac{1}{M^2}$ prescription in M^2. The final state hadronisation was obtained as that of a quark anti-quark pair in JETSET [22, 23], one of which scattered off the pomeron (momentum fraction $x_{quark/\gamma}$) and the other of which did not (momentum fraction $1 - x_{quark/\gamma}$). The resulting hadronic system of mass M then fills the available longitudinal phase space roughly uniformly, has a transverse momentum distribution which is limited exponentially ($e^{\sim -7p_T}$ in p_T^2), and has a charged multiplicity which is observed to follow approximately KNO scaling [24]. All these features are characteristic of soft diffractive dissociation in high energy hadron physics. No explicit hard hadronic scattering contribution was included in this model. All characteristics of the generated hadronic final state are very similar to those obtained using the diffractive option of PYTHIA [25, 23].

Deep inelastic electron–pomeron scattering was modelled using RAPGAP [26], a program in which the virtual photon interacts directly either with a quark constituent of the pomeron (figure 3e)) or via a quark loop with a gluon constituent - electron–pomeron scattering via photon–gluon fusion (figure 3f)). In both cases a remnant is left at low p_T with respect to the pomeron and hence also to the proton. The fragmentation of the partons involved in the hard sub-process and of the pomeron remnant were modelled using JETSET [22, 23]. In comparisons with data which follow, we consider two contrasting hypotheses for pomeron structure, namely either quark (figure 3 e)) or gluon (figure 3 f)) contributions. In each, the parton distribution functions $p(z)$ for the pomeron structure were taken to have the form $zp(z) \sim z(1 - z)$, where in the former $z = x_{quark/\!I\!P}$ is the fraction of the pomeron momentum carried by the struck quark, and in the latter $z = x_{gluon/\!I\!P}$ is the fraction of the pomeron momentum carried by the gluon, in the virtual photon pomeron interaction. Results from high p_T jet production in diffractive proton anti-proton interactions favour a hard distribution, such as that above, for $zp(z)$ [27], and in all comparisons we have found that the choice of a parton distribution function with a softer z dependence does not describe the data as well. It is also necessary for the gluon contribution to require a minimum momentum $\hat{p}_T$ transverse to the virtual photon for the final state partons. This ensures the validity of the perturbative matrix element calculations. In comparisons made here $\hat{p}_T > 1\,GeV$ was used. The phenomenological description of the pomeron was similar to that in the VMD–like model. The $x_{I\!P/p}$ distribution, where $x_{I\!P/p}$ is the fraction of the proton momentum carried by the pomeron $I\!P$, then follows a $\frac{1}{x_{I\!P/p}}$ distribution. At fixed Q^2, this results in a $\frac{1}{M^2 + Q^2}$ dependence in M^2.

---

[1] A recent measurement [19] gives $R_{LT} = 2.0 \pm 0.3$ at $< Q^2 >= 6\,GeV^2$ with no evidence for strong variation with Q^2 for $2 < Q^2 < 15\,GeV^2$ in diffractive production of $\rho(770)$ on nuclei.
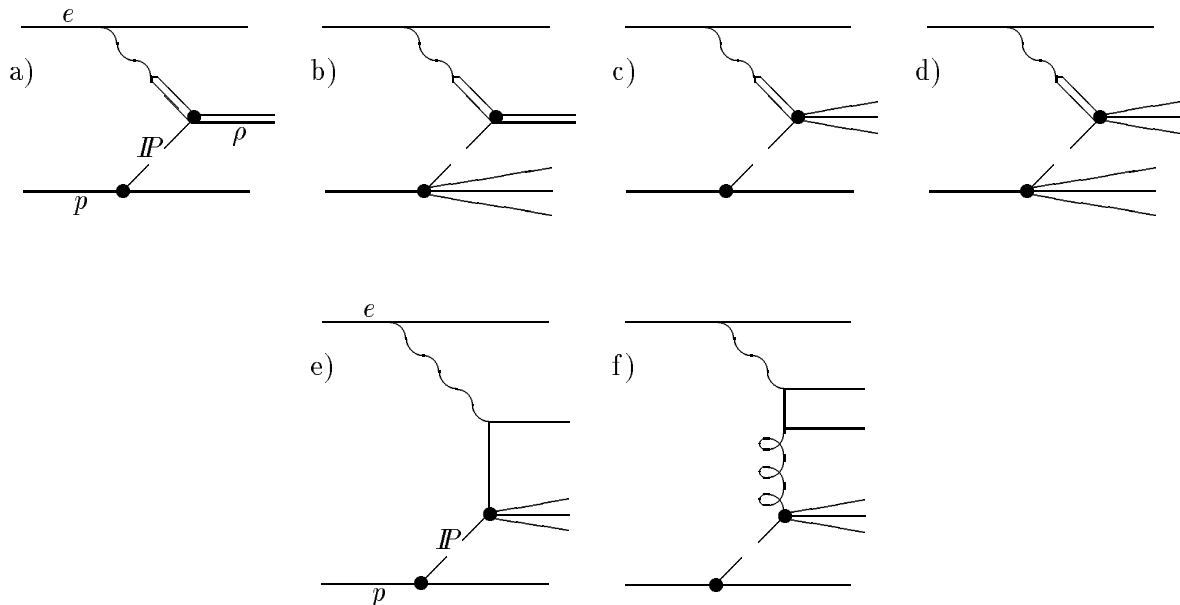
Figure 3: Diagrams which illustrate VMD–like and deep inelastic electron-pomeron scattering descriptions of rapidity gap events; a) ρ production via elastic VMD; b) VMD ρ production with soft dissociation of the proton; c) VMD photon interaction followed by soft dissociation of the vector meson; d) VMD photon interaction followed by soft dissociation of both the vector meson and the proton; e) inelastic $e\!I\!P$ scattering (off a quark in the pomeron); f) inelastic $e\!I\!P$ scattering (off a gluon in the pomeron via photon–gluon fusion); e) and f) are both leading twist electron-parton processes in QCD.

Both the VMD–like and the deep inelastic pomeron Monte Carlo programs included a full description of the QED electron–photon vertex but did not simulate initial or final state QED radiation.

Before making comparisons with our data, the events generated using the models above were passed through a full Monte Carlo simulation of biases due to acceptance, to measurement in H1, and to data analysis. No attempt is made in the following to correct measured distributions for these effects. In all comparisons, unless otherwise stated, the generated event yield from the diffractive physics simulations was normalised to the experimental yield of selected rapidity gap events, $\eta_{max} < 1.8$, after subtraction of the "tail" due to standard DIS events. All figures are shown with statistical errors only.

5 The Data and their Interpretation

5.1 The Data

As shown in figure 2, the data are observed to contain a larger number of events with small values of η_{max} than expected from standard DIS simulations. The rate of decrease of the η_{max} distribution at small η_{max} is less than at large η_{max}, indicating that different mechanisms are responsible for the production of hadrons in low and high η_{max} events. Figure 4 shows the scatter plot of the size of the largest measured pseudo-rapidity gap $\Delta\eta$ within the hadronic final state against the pseudo-rapidity of the forward edge of the gap, η_{end}. The gaps were required to be within the detector acceptance, that is $\eta_{end} \leq \eta_{LAr}$, and to have measured hadronic energy not in excess of $0.4\,GeV$. Rapidity gap events with small η_{max} (figure 2) appear as a distinct population with large pseudo-rapidity intervals $\Delta\eta$ devoid of significant hadronic energy extending to the
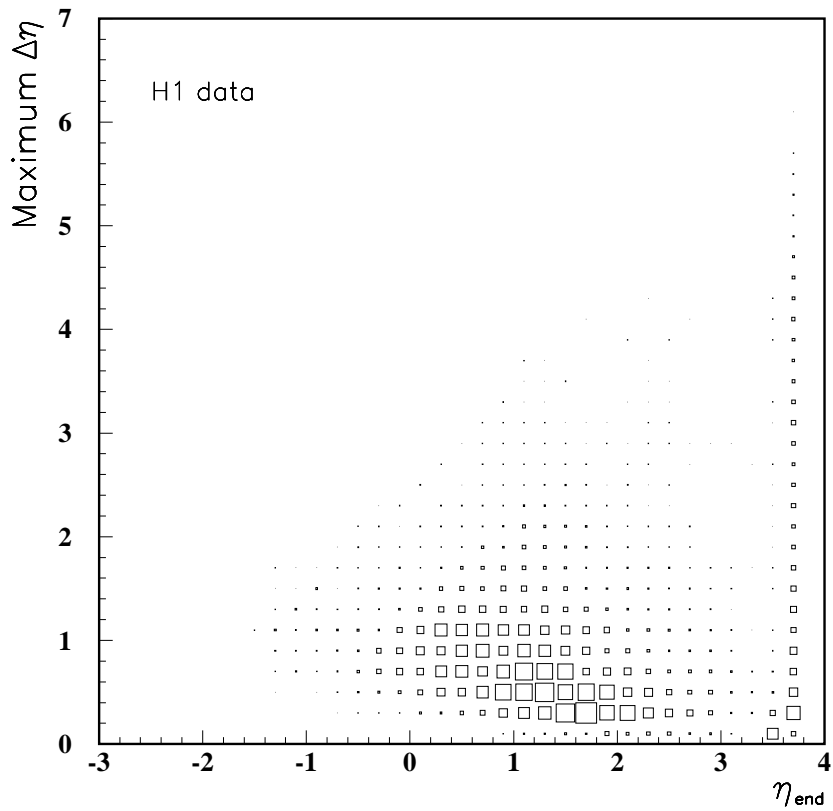
Figure 4: Scatter plot for all DIS events of the size of the largest observed interval of laboratory pseudo-rapidity which contains less than $0.4\,GeV$ hadronic energy $\Delta\eta$ against the most forward pseudo-rapidity η_{end} to which the interval can be measured ($\eta_{end} \leq \eta_{LAr}$ where η_{LAr} is the largest pseudo-rapidity which may be measured in the liquid argon calorimeter, namely ~ 3.65); note that the binning of the data necessarily follows that used in the determination of η_{max} explained in the text.

most forward measurable values $\eta_{end} \sim \eta_{LAr}$ (smeared according to the distribution of event vertices).

Of the 734 selected rapidity gap events, only 7% have energy deposition above threshold ($\sim 0.6\,GeV$) in the plug calorimeter, compared with 71% for the entire DIS sample. Including corrections for out of time segments originating from earlier or later ep bunch crossings, at least one track segment could be reconstructed in the Fμ drift chambers in only 16% of the rapidity gap events, compared with 73% for the entire DIS sample. Monte Carlo studies, which include a detailed modelling of the forward components of H1, both active and passive, and which reproduce well the observed response in the former, show that these results are consistent with diffractive processes in which the rapidity gap extends to $\eta = 6.6$ for a large proportion of the events. A similar comparison using P$_{tag}$ (19% with ≥ 1 hit for rapidity gap events, 43% for all DIS events), when taken together with the above Monte Carlo study, is consistent with proton diffractive dissociation in $\sim 30\%$ of rapidity gap events, which is similar to measurements of diffractive dissociation in $\bar{p}p$ interactions at comparable CM energy [28].

The rapidity gap events are distributed over the entire Q^2 and Bjorken-x range studied here, namely $5 < Q^2 < 120\,GeV^2$ ($< Q^2 >= 21\,GeV^2$) and $10^{-4} < x < 10^{-2}$ ($< x >= 0.0016$) [2] Figure 5a) shows the ratio R of rapidity gap events to all DIS events as a function of Q^2, reconstructed using the measured angle and energy of the scattered electron in the BEMC. The ratio $R(Q^2)$ is seen to decrease with increasing Q^2. This may not reflect the behaviour of the mechanism producing rapidity gap events because the use of the $\eta_{max} < 1.8$ criterion to select such events introduces a bias. Bjorken-x and Q^2 are correlated and events at larger x often have hadronic energy in the forward direction. The selection efficiency thus decreases with Q^2. Furthermore, in the diffractive hard scattering picture the selection efficiency depends sensitively on the behaviour of the pomeron remnant, on the pomeron momentum distribution, and on the pomeron parton distribution function. To minimise the effects of the selection bias due to energy associated with the struck object entering the forward rapidity gap region, we show in figure 5b) $R(Q^2)$ in different Bjorken-x regions. $R(Q^2)$ now has no significant dependence on Q^2, which is consistent with, but is not conclusive evidence for, a production mechanism for rapidity gap events which is leading twist in QCD.

The spectra of the invariant mass (M_X) of the measured hadronic final state for all rapidity gap events and for all DIS events are shown in figure 6. M_X is determined from energy deposition in cells of the liquid argon calorimeter. The M_X spectrum for the rapidity gap events peaks at $3.5\,GeV$ which is considerably lower than for all DIS events, suggesting that the former have a lower hadronic mass scale than the latter. Some, but not all, of this difference is attributable to the reduction in M_X due to the phase space restriction implicit in the rapidity gap selection. This is demonstrated in figure 6 by showing, for DIS events with $\eta_{max} > 1.8$, the M_X spectrum calculated ignoring calorimetric energy deposits with $\eta > 1.8$, that is energy deposits in the rapidity gap region. Above the peak at $3.5\,GeV$, the observed M_X spectrum for rapidity gap events is consistent with both the VMD and the RAPGAP (not shown) simulations, the former of which has built into it the characteristic $\frac{1}{M^2}$ distribution in the mass squared M^2 of any diffractively dissociating hadron.

The number of rapidity gap events in the sample with only two charged particles is 154 and in 123 of these the tracks have opposite sign and may arise from the decay of neutral vector mesons. In the above samples, 34 and 29 events respectively have less than $1.5\,GeV$ of energy deposited in the calorimeters which is not associated spatially with the charged particles. The latter 29 events (4% of all selected rapidity gap events) are candidates for exclusive VM production. Calorimeter energy was considered to be associated with a charged particle if it was within a cylinder about the particle direction of radius $15\,cm$ in the electromagnetic section

---

[2]Note that the event selection described in sections 2 and 3 is made using electron scattering angle and energy. The ranges quoted for Q^2 and Bjorken-x each correspond to the maximum accessible in the selected data.
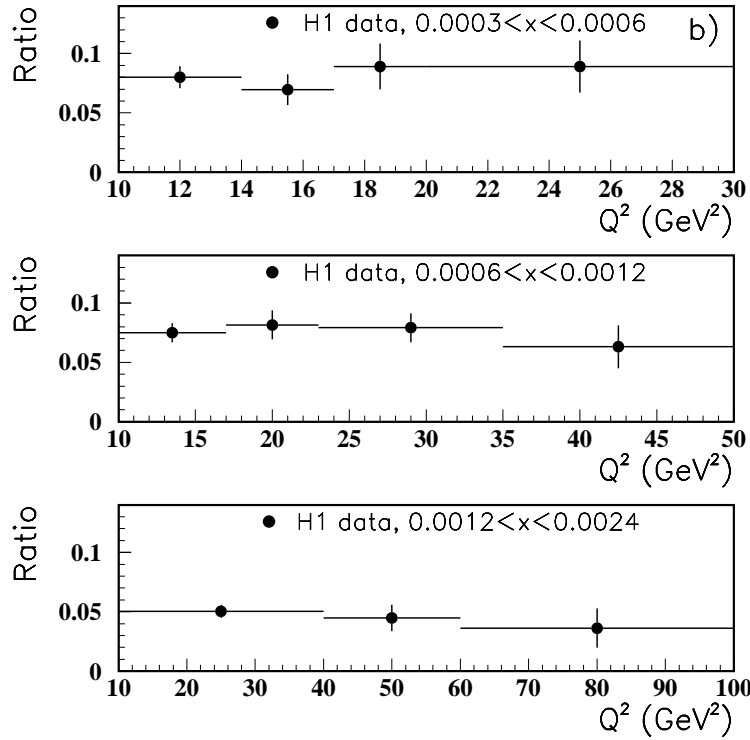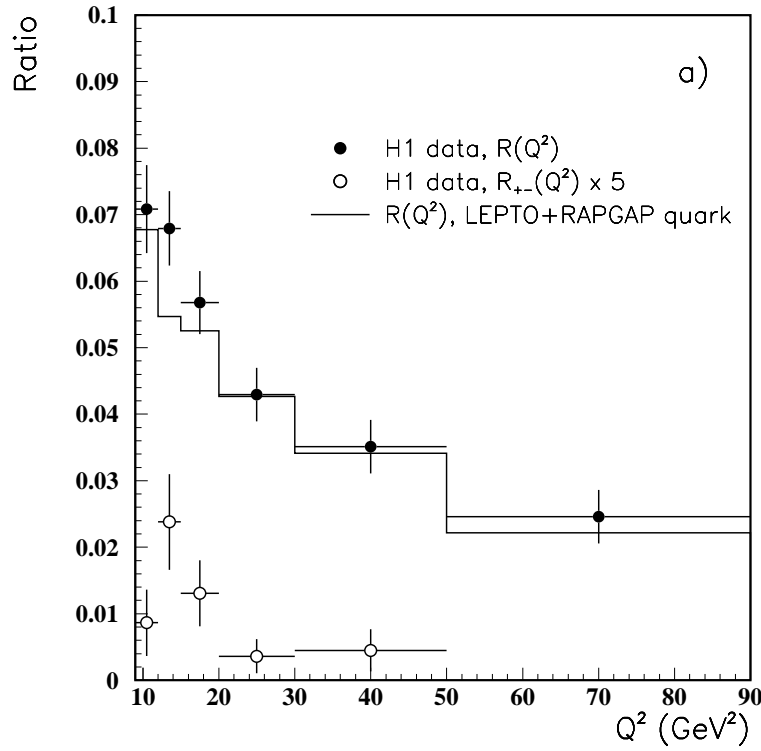
Figure 5: a) The ratio of rapidity gap events to all DIS events (R in text) and the ratio of rapidity gap events which are candidates for exclusive production of $\rho(770)$ to all DIS events (R_{+-} in the text scaled by a factor 5 for display purposes) both as functions of Q^2; also shown is the expectation for $R(Q^2)$ for the RAPGAP model assuming quark sub-structure in the pomeron; b) $R(Q^2)$ for different Bjorken–x ranges.
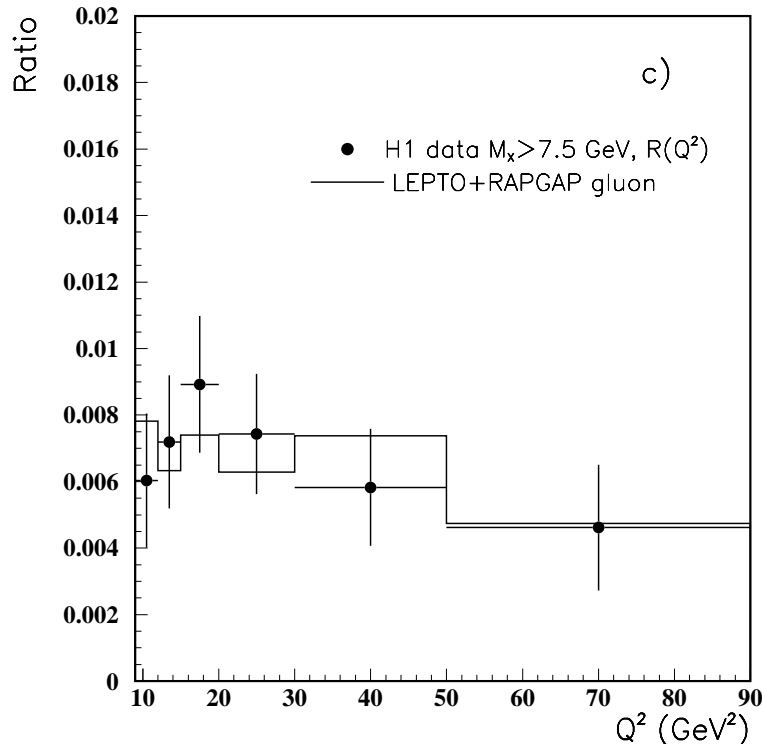
14

Figure 5: c) $R(Q^2)$ for events with $M_X > 7.5\,GeV$; the expectation from RAPGAP assuming gluon sub-structure in the pomeron is also shown.

of the liquid argon calorimeter, $25\,cm$ in the hadronic section, and $15\,cm$ in the BEMC. The two charged particle mass spectrum, assuming both particles are pions, is shown in figure 7 a). There is evidence for exclusive $\rho(770)$ production with relatively little signal at higher mass. It is compatible with measurements of $\rho(770)$ photoproduction and lower Q^2 electroproduction [16] and with the expectation from the simulation of exclusive VM production (normalised to the observed 29 events). Figure 7b) shows the η_{max} spectrum for these events which is also seen to be consistent with the expectations of exclusive VM production. The ratio R_{+-} of these candidate events for exclusive $\rho(770)$ in the rapidity gap sample to all DIS events is shown in figure 5 a) as a function of Q^2. It shows no evidence, albeit with limited statistical sensitivity, for any substantial difference from all rapidity gap events. Note that it is unlikely that this $\rho(770)$ production is due to any remaining electron beam gas events in the rapidity gap sample because about two thirds of the candidate $\rho(770)$ events are kinematically incompatible with the assumption that they originate from beam gas interactions.

From the full simulation of acceptance, measurement and data selection biases in H1, we estimate our efficiency for selecting exclusive vector meson events (primarily $\rho(770)$ with small contributions from the kinematic reflections associated with $\omega(783)$ and $\phi(1020)$ production) from the sample of rapidity gap events to be $\sim 50\%$. Thus the proportion of exclusive $\rho(770)$, $\omega(783)$ and $\phi(1020)$ events in the latter sample is $\sim 10\%$. There is no evidence for a similar proportion of exclusive $\rho(770)$ production in the DIS two track events with $\eta_{max} > 1.8$.

5.2 Comparison with VMD-like Physics

The shapes of both the observed η_{max} distribution (figure 8 a)), and the observed M_X spectrum (figure 6) can be reproduced using the VMD motivated simulation (normalised to the total
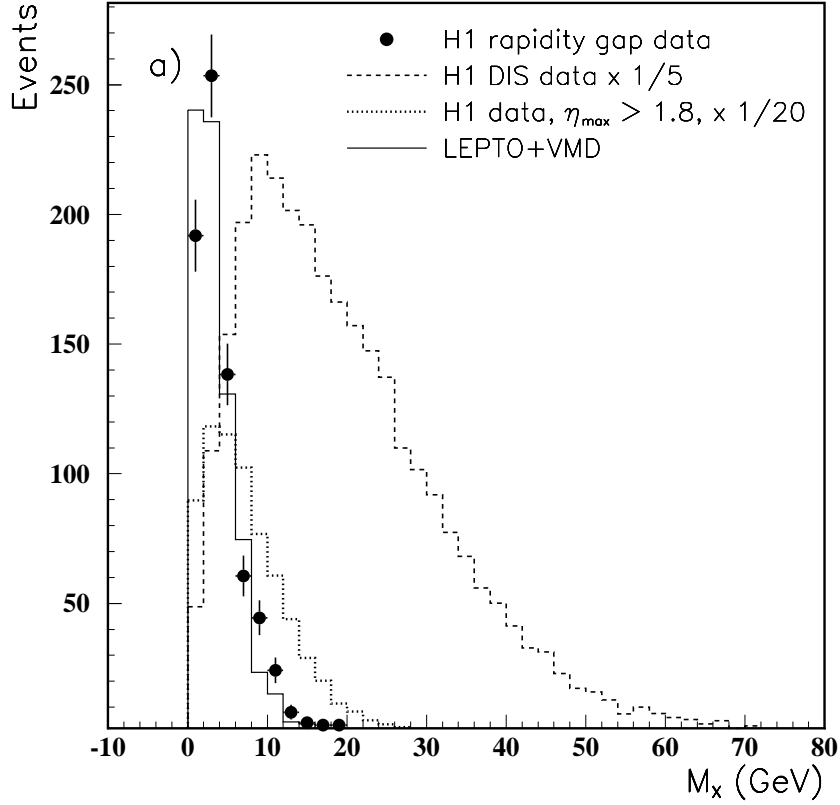
Figure 6: Invariant mass spectrum of the measured hadronic final state for rapidity gap events, for DIS events (scaled by a factor $\frac{1}{5}$ for display purposes), and for DIS events with $\eta_{max} > 1.8$ omitting energy deposits with $\eta > 1.8$ from the mass calculation (scaled by a factor $\frac{1}{20}$ for display purposes): the solid line is the expectation of the VMD–like simulation described in the text for the rapidity gap data, with a small contribution from LEPTO.
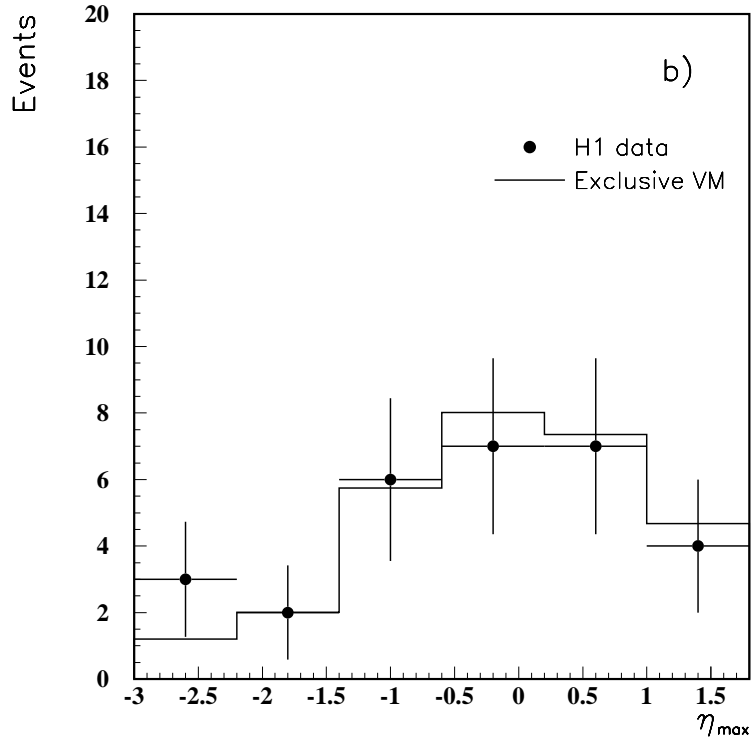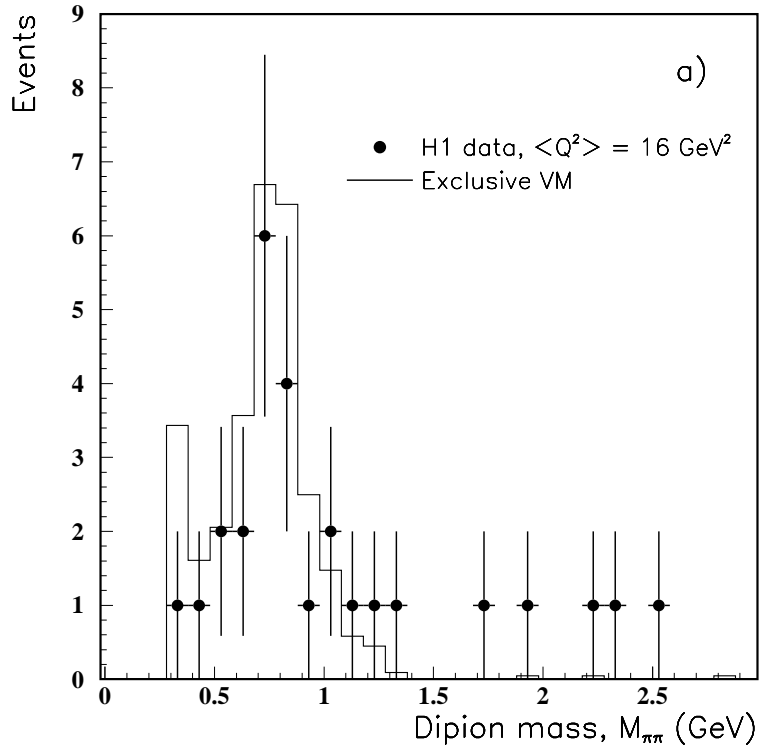
16

Figure 7: a) Dipion mass spectrum for oppositely charged two track rapidity gap events with less than $1.5\,GeV$ additional energy which is not associated with the tracks; the solid line is the expectation from exclusive VM production described in the text. b) η_{max} spectrum for the events in a) together with the expectation from the simulation of exclusive $\rho(770)$ production.

number of rapidity gap events selected) and LEPTO. Both distributions obtained from the model are dependent on the proportions of exclusive VM (ρ, ω and ϕ) and of dissociative VMD–like diffractive events (figure 3) both with or without proton dissociation, and, to a lesser extent, on the understanding of the "tail" due to standard DIS processes. The VMD expectation for the η_{max} spectrum which is shown in figure 8 a) has the proportion of observed events attributable to exclusive VM (with or without proton dissociation) consistent with observation above, namely 10%. Using our forward detectors (see section 3 above), we estimate that $\sim 30\%$ of events with $\eta_{max} < 1.8$ involve proton diffractive dissociation. The fraction of events which may be attributed to exclusive VM production is thus small when compared with photoproduction measurements ("elastic" VM production cross section $= 18 \pm 7\,\mu b$, total γp diffractive cross section $= 33 \pm 8\,\mu b$ [29]). Given the uncertainties in the Q^2 dependences both of elastic and of inelastic production in VMD–like processes (and thus also their experimental acceptance), the hypothesis that the rapidity gap data are attributable solely to such processes cannot be rejected. The uncertainties in the Q^2 dependence of the VMD model mean it is possible to reproduce the observed $R(Q^2)$ in figure 5 in a VMD–like picture by an appropriate choice of the ratio of longitudinal to transverse virtual photon-proton total cross sections (R_{LT} in equation 1), or also by means of a different VMD-motivated choice for $F(Q^2, y)$ [6].

The yield of two charged particle events in figure 7 is in agreement with the VMD expectation of exclusive electroproduction of $\rho(770)$, $\omega(783)$ and $\phi(1020)$. We estimate the total elastic photoproduction cross sections at our mean W of $130\,GeV$ by extrapolating values from low energy ($W \sim 10$ to $15\,GeV$) [30]. The prescription used describes the high energy behaviour of the total photoproduction cross section [31, 29], namely $\propto W^{2\Delta}$ with $\Delta = 0.0808$ [21] and predicts a rise of the $\rho(770)$ "elastic" production cross section $\propto \frac{W^{4\Delta}}{b}$ where b specifies the t dependence of the cross section ($\frac{d\sigma(ep \to e\rho p)}{dt} \propto e^{bt}$) and b is assumed to increase logarithmically with W. We then estimate a $\rho(770)$ yield of $\sim 20\,(230)$ events in figure 7a), where the two estimates correspond to the choices $R_{LT} = 0\,(\frac{Q^2}{m_V^2})$ in equation 1. Note that the uncertainties due to ignorance of R_{LT} for each VM contribution far outweigh the uncertainties in the photoproduction cross sections due to extrapolation to HERA energy, due to the contribution from inelastic VM production with unseen proton dissociation, and due to any remaining uncertainties in our simulation of experimental bias and acceptance [3].

If the VMD–like interpretation of the rapidity gap events is correct, then, using the model as specified above, the total diffractive contribution amounts to approximately 15% of the total observed DIS data sample ($5 < Q^2 < 120\,GeV^2$, $10^{-4} < x < 10^{-2}$).

5.3   Comparison with Deep Inelastic Electron-Pomeron Physics

The hypothesis of deep inelastic electron–pomeron scattering as implemented in the RAPGAP model is in good agreement with observation in the kinematic region where it is applicable. The rapidity gap and M_X distributions depend on the pomeron parton distribution functions used, on the pomeron momentum distribution, and, for the gluon component, on the $\hat{p_T}$ cut used. The former two are taken as specified in section 4 above. The effect of the latter on the M_X distribution is small for $M_X > 7.5\,GeV$. Figure 8 b) shows that the shape of the observed η_{max} distribution (normalised to the observed number of rapidity gap events) is well reproduced by the sum of the RAPGAP and DIS simulations, assuming quark pomeron sub-structure. Similar agreement is observed in figure 8 c) where the observed η_{max} distribution for $M_X > 7.5\,GeV$ is

---

[3]Using the recent determination of $R_{LT} = 2.0 \pm 0.3$ in the diffractive muoproduction of $\rho(770)$ on nuclei at large Q^2 ($2 < Q^2 < 15\,GeV^2$) in the VMD–like picture in section 4, we estimate a yield of about 60 exclusive vector meson ($\rho(770) + \omega(783) + \phi(1020)$) in our data, in good agreement with observation including the described selection efficiency correction.
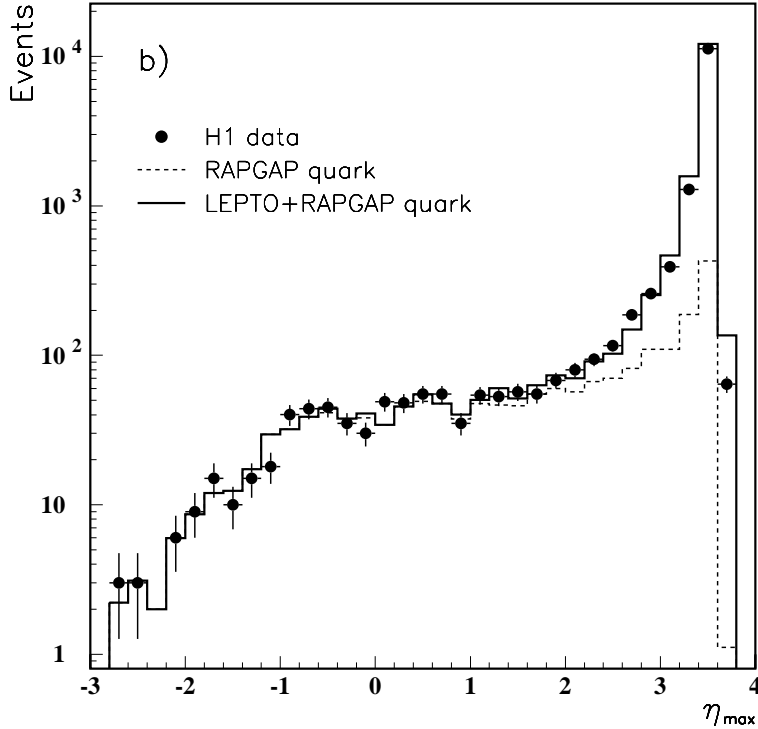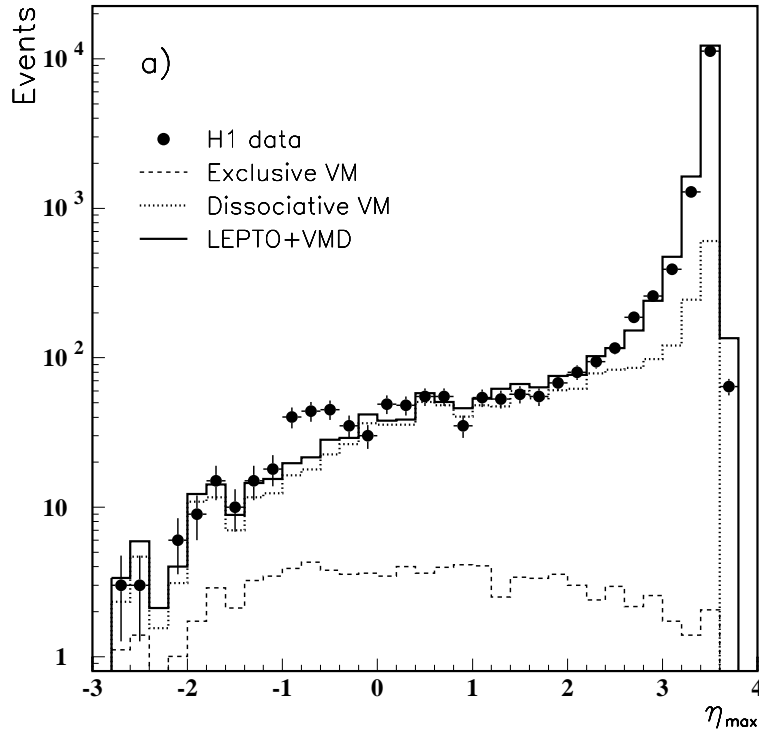
Figure 8: a) Distribution of measured η_{max} for all DIS events together with the VMD expectation; shown are the contributions from exclusive ρ, ω and ϕ production (exclusive VM) from inelastic production (dissociative VM) and from the sum of total VMD and LEPTO. b) Distribution of measured η_{max} for all DIS events with the expectations from RAPGAP assuming a quark parametrisation for the pomeron structure function (see text), and from the sum of LEPTO and RAPGAP.
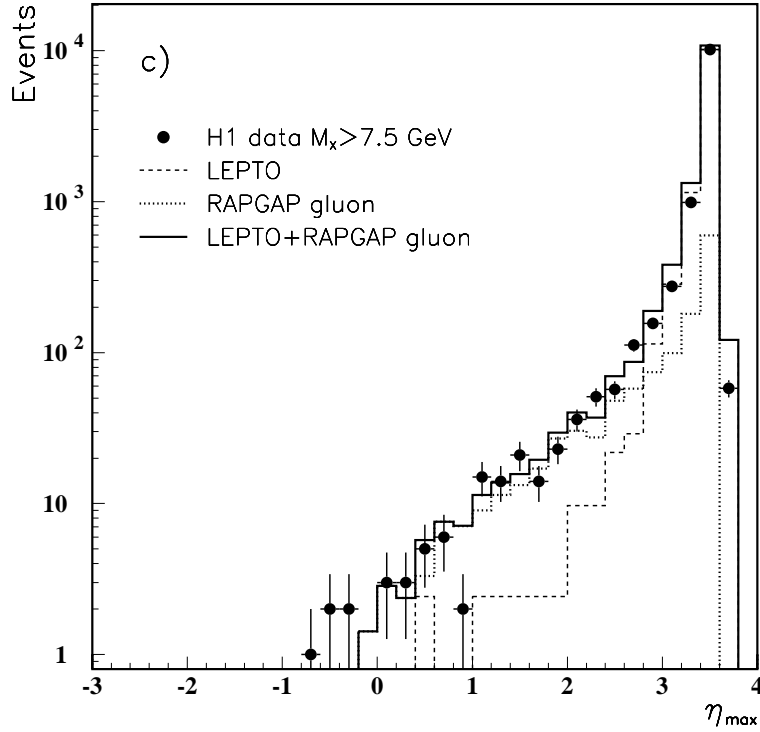
Figure 8: c) Distribution of measured η_{max} for all DIS events with measured invariant mass $M_X > 7.5\,GeV$ with the expectations from LEPTO, from RAPGAP assuming a hard gluon parametrisation for the pomeron structure function (see text), and from their sum.
In a) b) and c) above, the normalisations of VMD and RAPGAP are such that each reproduces the number of observed DIS events with $\eta_{max} < 1.8$.

compared with the sum of the RAPGAP and DIS simulations, assuming gluon pomeron sub-structure (normalisation is again to the number of selected rapidity gap events). The observed Q^2 dependence of the yield of rapidity gap events (in the form of $R(Q^2)$ in figures 5 a) and c)) is as expected for the RAPGAP simulation both for quark (figure 5 a)) and for gluon (figure 5 c)) pomeron sub-structure.

If the ansätze in the RAPGAP model of deep inelastic electron pomeron scattering, namely the descriptions of the pomeron flux, its parton structure $zp(z)$, the perturbative calculation of the DIS photon-parton processes, and the hadronisation of both the current and the remnant from the pomeron, are correct, then $\sim 13\%$ of our observed DIS events are attributable to inelastic diffraction in the kinematic range of these data ($5 < Q^2 < 120\,GeV^2$, $10^{-4} < x < 10^{-2}$) assuming the pomeron to be composed primarily of quarks. If the pomeron is considered to be composed of gluons this proportion becomes $\sim 10\%$ of our observed DIS events with $M_X > 7.5\,GeV$.

5.4   Discussion

If the observed deep inelastic rapidity gap events are attributed to a diffractive process, then, with the exception of the evidence for exclusive VM production, all features are very well described by the RAPGAP model. A description in terms of processes which do not involve the resolution and spatial separation of colour in VMD–like elastic and inelastic electroproduction (with or without proton dissociation) is also possible. The observation of evidence for exclusive VM production in the selected sample of rapidity gap events ($\sim 10\%$ of selected events after correction for selection losses) and the fact that the yield is broadly consistent with extrapolated measurements of electroproduction at lower Q^2 suggests that VMD–like processes do contribute at some level to the physics of rapidity gap events.

Note that, despite the acceptable overall description of the data obtained, uncertainties remain in this picture. The possibility of a contribution to rapidity gap events from non-diffractive processes such as neutral or charged meson exchange, or from models such as that in [32], cannot yet be excluded. The partonic interpretation of the pomeron structure function $zp(z)$ is complicated by the possibility of a contribution from VMD-like processes.

6   Summary

From an integrated ep luminosity at HERA of $273\,nb^{-1}$ we have reported the observation of a sample of 734 deep inelastic ep scattering (DIS) events at low Bjorken–x ($5 < Q^2 < 120\,GeV^2$, $10^{-4} < x < 10^{-2}$) with a large pseudo-rapidity interval around the forward proton direction which is devoid of significant hadronic energy flow. Present descriptions of DIS in terms of electron interactions with the partonic structure of the proton and appropriate parton hadronisation do not predict such "rapidity gap" events.

The observed distributions of maximum pseudo-rapidity of hadronic energy deposition η_{max}, of M_X, and of the Q^2 dependence of the observed yield as a fraction R of total DIS events, are all well described in terms of diffractive exchange in which the coloured partonic sub-structure of this exchange is resolved and spatially separated – deep inelastic electron–pomeron scattering.

Evidence for exclusive VM production, amounting to about 10% of all selected rapidity gap events ($\eta_{max} < 1.8$), is observed in such events with only two oppositely charged particles, suggesting that at least some of the rapidity gap sample may involve the diffractive interaction of the virtual photon via a vector meson dominance like (VMD–like) mechanism. An interpretation, quantified in the framework of VMD, in which all the rapidity gap events are attributed to

interactions in which the virtual photon and proton interact diffractively without any resolution and spatial separation of the coloured sub-structure of the exchanged object also describes the data well. If such a VMD-like interpretation alone is valid, then the proportion of "elastic" events is small.

7 Acknowledgments

We are grateful to the HERA machine group whose outstanding efforts have made and continue to make this experiment possible. We appreciate the immense effort of the engineers and technicians who constructed and maintain the H1 detector. We thank the funding agencies for financial support. We acknowledge the support of the DESY technical staff. We also wish to thank the DESY directorate for the hospitality extended to the non-DESY members of the collaboration. We thank J. Bartels and G. Ingelman for helpful discussions.

References

[1] I. Abt et al. (H1 Collaboration) "Energy Flow and Charged Particle Spectra in DIS at HERA", DESY preprint 94-033 (1994), submitted to Zeit. Phys. **C**.

[2] M. Derrick et al. (ZEUS Collaboration) Phys. Lett. **B315** 481 (1993),
M. Derrick et al. (ZEUS Collaboration) "Observation of jet production in deep inelastic scattering with a large rapidity gap at HERA" DESY preprint DESY 94-063 (1994).

[3] W. Bartel, "$\sigma_{\gamma p}^{tot}$ and Diffractive Processes in Photoproduction and DIS.", in Proc. of the Europhysics Conference, Marseilles, France, July 1993, ed. J. Carr and M. Perrottet, p. 585.
J. B. Dainton, "Results from the H1 Experiment at HERA.", in Proc. XVI International Symposium on Lepton Photon Interactions, Cornell, Ithaca, USA, August 1993, ed. P. Drell and D. Rubin, p. 87 and Rutherford Appleton Laboratory preprint RAL 94-12.
A. De Roeck, "Results from the H1 Experiment.", in Proc. of the Europhysics Conference, Marseilles, France, July 1993, ed. J. Carr and M. Perrottet, p. 791 and DESY preprint DESY 94-005 (1994).

[4] J. J. Aubert et al. (EMC collaboration) Phys. Lett. **B161** 203 (1985).

[5] P. Amaudruz et al. (NMC collaboration), Zeit. Phys. **C54** 239 (1992).

[6] J. J. Sakurai, Phys. Rev. Lett. **22** 981 (1969)
J. J. Sakurai and D. Schildknecht, Phys. Lett. **40B** 121 (1972).

[7] A. Donnachie, P. Landshoff, Phys. Lett. **B185** 403 (1987).

[8] J. D. Bjorken, "Hadron Final States in Deep Inelastic Processes", in "Current Induced Reactions: International Summer Institute in Theoretical Particle Physics in Hamburg 1975", ed. J. G. Kröner, G. Kramer, and D. Schildknecht, Lecture Notes in Physics, Springer Verlag, 1976.

[9] I. Abt et al. (H1 Collaboration), "The H1 Detector at HERA", DESY preprint DESY 93-103 (1993).

[10] B. Andrieu et al. (The H1 Calorimeter Group), Nucl. Inst. Meth. **A336** 460 (1993).

[11] I. Abt et al. (H1 Collaboration), Nucl. Phys. **B407** 515 (1993).

[12] Ch. Berger et al. (PLUTO Collaboration), Zeit. Phys. **C26** 353 (1984).

[13] G. Ingelman, "LEPTO 6.1", unpublished program manual.
H. Bengtsson, G. Ingelman and T. Sjöstrand, Nucl. Phys. **B301** 554 (1988),
G. A. Schuler and H. Spiesberger, Proc. of the Workshop "Physics at HERA", p 1419, ed.
W. Buchmüller and G. Ingelman, Hamburg (1991).

[14] L. Lönnblad, Comput. Phys. Commun. **71** 15 (1992).

[15] A. D. Martin, W. J. Stirling and R. G. Roberts, Phys. Lett. **B306** 145 (1993), ibid. **B309** 492 (1993).

[16] T. H. Bauer, R. D. Spital, D. R. Yennie, F. M. Pipkin, Rev. Mod. Phys. **50** 261 (1978).

[17] B. List, "Diffraktive $J/\psi-$Produktion in Elektron-Proton-Stößen am Speicherring HERA", Diploma Thesis (Tech. Univ. Berlin), 1993 (unpublished).

[18] P. Joos et al. Nucl. Phys. **B113** 53 (1976),
P. Joos et al. Nucl. Phys. **B122** 365 (1977).

[19] A. Sandacz, (NMC collaboration), "Exclusive ρ^0 and ϕ Muoproduction at Large Q^2", paper gls0267 submitted to the 27th International Conference on High Energy Physics, Glasgow, UK, July 1994.

[20] K. Goulianos, Phys. Rep. **101** 169 (1983).

[21] A. Donnachie, P. Landshoff, Phys. Lett. **B296** 227 (1992).

[22] T. Sjöstrand, CERN preprint CERN-TH-6488-92 (1992).

[23] T. Sjöstrand, Comput. Phys. Commun. **43** 367 (1987).

[24] Z. Koba, H. B. Nielsen, P. Oleson, Nucl. Phys. **B40** 317 (1972).

[25] H.-U. Bengtsson and T. Sjöstrand, Comput. Phys. Commun. **46** 43 (1987).

[26] H. Jung, "Hard Diffractive Scattering in High Energy ep Collisions and the Monte Carlo Generator RAPGAP", DESY preprint DESY 93-182 (1993), submitted to Comput. Phys. Commun.

[27] A. Brandt et al. (UA8 Collaboration), Phys. Lett. **B211** 239 (1988)
A. Brandt et al. (UA8 Collaboration), Phys. Lett. **B297** 417 (1992).

[28] S. Belforte (CDF Collaboration), "Measurement of the Elastic, Total, and Diffraction Cross Sections at Tevatron energies", in Proc. of the Europhysics Conference, Marseilles, France, July 1993, ed. J. Carr and M. Perrottet, p.578, July 1993, and Fermilab preprint Fermilab-Conf-93/358-E (1993).

[29] M. Derrick et al. (ZEUS Collaboration), "Measurement of the Total and Partial Photon Proton Cross Sections at $180\,GeV$ center of mass energy", DESY preprint DESY 94-032 (1994), submitted to Zeit. Phys. **C**,
M. Derrick et al. (ZEUS Collaboration), Phys. Lett. **B293** 465 (1992).

[30] D. Aston et al., Nucl. Phys. **B209** 56 (1982)
M. Atkinson et al., Nucl. Phys. **B231** 15 (1984),
J. Busenitz et al., Phys. Rev. **D40** 1 (1989),
R. M. Egloff et al., Phys. Rev. Lett. **43** 657 (1979).

[31] T. Ahmed et al. (H1 Collaboration), Phys. Lett. **B299** 374 (1993).

[32] W. Buchmüller, "Probing Lumps of Wee Partons in Deep Inelastic Scattering", DESY preprint DESY 94-107 (1994).